Forensic Science International 266 (2016) 54–62

Contents lists available at ScienceDirect

Forensic Science International

journal homepage: www.elsevier.com/locate/forsciint

The impact velocity and bone fracture pattern: Forensic perspective

Haim Cohen [a,b,*], Chen Kugel [b,c], Hila May [a], Bahaa Medlej [a], Dan Stein [a], Viviane Slon [a,1], Israel Hershkovitz [a], Tamar Brosh [d]

[a] Department of Anatomy and Anthropology, Sackler Faculty of Medicine, Tel Aviv University, Tel Aviv 69978, Israel
[b] National Center of Forensic Medicine, Tel Aviv 61490, Israel
[c] Sackler Faculty of Medicine, Tel Aviv University, Tel Aviv 69978, Israel
[d] Laboratory of Fine Measurements, Dental School of Medicine, Tel-Aviv University, Israel

ARTICLE INFO

Article history:
Received 20 August 2015
Received in revised form 6 February 2016
Accepted 26 April 2016
Available online 7 May 2016

Keywords:
Bone
Fracture
Pattern
Impact
Velocity
Forensic

ABSTRACT

Studies on bone-energy interaction are meager and revealed only a general correlation between the fracture pattern and the mechanism of the insult.

This study has two objectives, to establish a usable fracture analysis method and to reveal the association between the energy of the force and the fracture pattern. Dynatup Model POE 2000 (Instron Co.) low energy pendulum impact machine was utilized to apply impact loading on fresh pig femoral bones ($n = 30$). The bone clamp shaft was adjusted to position the bone for three-point bending with additional bone compression. Three different velocities of the forced applied were carried out. On average, the number, length and the curviness of the fracture lines created under moderate and high-energy impact is significantly higher compared to a low-energy impact. Most fractures lines were located on the impacted aspect in bones subjected to moderate- and high-velocity impact. Four oblique-radial fracture lines running from the point of impact creating a double butterfly pattern were found in bones subjected to moderate and high-velocity impact. Only "false" wedge-shaped (butterfly) fragments were found in the current study. Our results suggest an association between fracture pattern and the velocity of the impact.

1. Introduction

Bone trauma is an important source of information regarding the circumstances that "led" to the death of the victim [1]. Proper fracture interpretation may assist in identifying the location and number of impact sites, establishing the sequence of blows, and determining the characteristics of the object that inflicted the injuries [2,3]. Studies on fracture pattern in the forensic setting are of importance in cases such as homicidal assault, suicide, falls, child abuse, and road traffic accidents. Knowledge on fracture associated with specific modes of trauma can be used to predict the nature of the injury. For example, in cases where homicidal victims and child abuse are suspected, identifying the fracture type may assist in determining the direction of the force and whether the bone was twisted or angulated. In the case of suspected fall, analysis of the fracture pattern may assist in determining the type of fall (simple fall or fall from a height), the surface of the impact, and in some cases, the landing orientation of the victim [4]. Analysis of fracture pattern could also be a useful tool for accident reconstruction purposes [5]. There are a limited number of loading modes to which bone can be subjected, and these results in predictable fracture patterns [6]. These patterns are usually classified into 6 classic types: transverse, oblique or butterfly, spiral, segmental and comminuted. This classification of fracture patterns is derived largely from the medical literature where determination of the stability of the injury, probable extent of associated soft tissue damage, and the prognosis for recovery are the primary motivations [7]. Transverse fracture runs at approximately right angles to the long axis of the long bone [8]. This fracture type can be the result of force producing bending [9] or severe angulations, but not necessarily under compression from the normal weight-bearing functions [7], or the result of force producing tension [10]. Transverse fractures become increasingly more comminuted as a result of direct trauma with progressively greater force. Completed and displaced transverse fractures often

* Corresponding author: Dr. Haim Cohen, Department of Anatomy and Anthropology, Sackler Faculty of Medicine, Tel Aviv University, Tel Aviv 69978, Israel. Tel.: +972 3 6409495; fax: +972 3 6408287.
E-mail addresses: haimcoh1@post.tau.ac.il (H. Cohen), chen.kugel@forensic.health.gov.il (C. Kugel), hilamay@gmail.com (H. May), Bahaamedlej@gmail.com (B. Medlej), maadan@gmail.com (D. Stein), slonviviane@gmail.com (V. Slon), anatom2@post.tau.ac.il (I. Hershkovitz), tbrosh@post.tau.ac.il (T. Brosh).
[1] Department of Evolutionary Genetics, Max Planck Institute for Evolutionary Anthropology, 04103 Leipzig, Germany.

http://dx.doi.org/10.1016/j.forsciint.2016.04.035
0379-0738/

result from mechanisms of high energy, such as injuries involving encounters with cars or falls from significant heights [9]. Oblique fractures run diagonally across the diaphysis with short blunt fractures usually ending at a 45° angle with no vertical segment [8,10]. An oblique fracture usually results from the combination of angulation and axial compressive forces of moderate intensity [7] or a combination of torsion and bending (when bending is the dominant loading) [11]. The fracture morphology reflects the predominant loading type (a long oblique is common when torsion is the predominant force or short oblique when the predominant force is bending or compression) [9]. The more common patterns are oblique transverse and butterfly fractures (or indirect wedge-shaped fractures) where the initial fracture is perpendicular to the long axis (representing the failure in tension), while the latter portion is oblique (representing the compression failure). Oblique-transverse and butterfly fractures are commonly seen in the lower extremities when the thigh or calf receives a lateral blow involving weight, as in the case of pedestrians injured by automobiles [10]. Butterfly fractures usually occur at low speed of impact. At higher speeds of impact, "dynamic" noncharacteristic transverse or multifragment fractures are usually observed [4]. Few words about Butterfly fracture are due here as this type of fracture is commonly used in forensic cases for establishing the position of a pedestrian in relation to a motor vehicle [15]. The mechanism of this fracture was the subject matter of Messerer's study in the late 19th century [16]. The rules put forward by him concerning the location of the base of the wedge (from the impact side) and its apex (according to the force direction) has become, from the early 60th of the previous century, a 'standards' in forensic medicine and is treated almost dogmatically both in the literature (especially textbooks) and in practice [15,22–25]. This is surprising considering the growing evidence to suggest the presence of a reversed phenomenon, i.e., the apex and not the base is directed toward the impact site ("false butterfly fracture"), in some of the cases. For example: Spitz and Russell [12] in their study on pedestrian leg impact found that in some cases, even a "false" wedge-shaped fragment may be seen. This observation was repeated by other studies [4,13,14,20]. Rich [4] claimed that a typical bending fracture (Messerer's wedge) can indicates the direction of impact only when the bone was bent at the moment of impact [4]. Already in 1963 Patscheider proved experimentally the possibility of the occurrence of "false" indirect wedge-shaped tibial and femoral fractures by hitting rigidly fixed human and animal bones with weighted pendulum [18]. On 1999 Teresinski and Mydro examined 14 femurs with wedge-shaped fractures following pedestrians' car accidents to evaluate the evidential value of wedge-shaped fractures: in only 50% of the cases a "true" wedge fractures ("Messerer's fractures") were found, 21% of the cases manifested "false" wedge fractures and the rest had the wedge at the impact side [15]. Spiral fractures are caused by rotational forces on the bone [7] or a combination of torsion and bending (when torsion is the dominant loading) [4]. These fractures tend to be the result of low-velocity forces [7] and were produced only from torsional loading in experimental testing of human cadaver long bones [5]. Torsion creates a state of pure shear between parallel transverse planes. In other planes (at other angles with respect to the longitudinal axis), tensile and compressive stresses are present, and they become maximum at a 45° angle to the longitudinal axis [17]. The fracture has long, sharp, pointed ends and vertical segment, which is the last component to form [10], in contrast to the ends of bones in oblique fractures, which are short, blunt and rounded [4]. The direction of the spiral indicates the direction of the torsional forces [10] and can be used to reconstruct the events that produced the fracture [7]. When multiple fractures leave diaphyseal portions separated from the proximal or the distal ends, the intervening segment is called a segmental fracture. This defect may result from multiple simultaneous fractures as would occur when a bone is hit at two points or by a large surface [7]. A comminuted fracture is one in which more than two fragments are generated [8] and usually results from relatively high levels of force [10]. Such fractures are most common in the lower extremity, which is often weight-bearing at the time of impact by an extraneous object. They are commonly seen in the legs of pedestrians hit by motor vehicles. The ability to distinguish between fracture patterns in bones following an impact at different velocities is extremely important. The need for traffic accident reconstruction is of major importance, since road traffic injuries are the leading cause of death worldwide among young people aged 10–24 years (World Health Organization) [27]. Analyses of the lower-extremity fracture patterns are particularly relevant in car-to-pedestrian impacts, since they reflect the actual location of the pedestrian relative to the vehicle and can shed light on the speed of the car when this is in question. It is well known that the greater the magnitude of the force, the higher its energy content, and hence, the more bone destruction. Conversely, the more complex the fracture pattern the greater the energy needed to produce the fracture [10]. A high-energy direct blow to an adult bone will cause a markedly comminuted fracture [13,29] typically associated with extensive soft tissue injury and indicating a large amount of energy dissipation in conjunction with a rapid loading rate [9,30]. Tissues surrounding bone, including muscle, tendons, ligaments, fat, and skin, can affect the fracture pattern by absorbing some of the load energy and also by creating additional load [6]. Studies on bone-energy interaction revealed only a general correlation between the fracture pattern and the mechanism of the insult [31] (cited from Rich [4]). Attempts to determine the crash speed on the basis of the severity of injuries were reported in a text book however this report has yielded no reliable methods of crash speed determination [32]. Text books on bone trauma mostly describe and define fracture types in relation to the direction of loading and loading type applied [7,8,10,33,34]. Studies on the association between the mechanical properties of the bone and physical injury concentrated mainly on microcracking behavior, their location, initiation and propagation [35–39]. These studies however did not explain the correlation between the macrocracking behavior on a whole bone in relation to different types of force applied. Any attempt to predict the behavior of a skeletal region under loading must reflect both the material properties of the bone in that region and its structure [40]. Although there is a consensus regarding the mechanism that produces certain fracture pattern, there are clearly competing theories in the medical literature in relation to others. In addition, most studies analyzing fracture patterns in 3-point bending did not include additional axial compression loading as when the thigh receives a lateral blow during weight bearing, as in the case of pedestrians injured by vehicles. In addition, the information regarding whether the bones were complete or partial during testing, and the precise site of impact is uncertain. Fracture pattern analysis can be a complicated process especially since in most cases the fracture pattern is far from being classic. The determination of the mechanism that results in particular patterns is better approached through experimentation rather than theorizing. Unfortunately, many unsubstantiated theories have been repeated and referenced for decades. Most studies that looked into the micro-morphology of fractures were performed by engineers who were interested in exploring the mechanical properties of bones. Physicians, on the other hand, were more interested in the macro-morphology of fractures (classification of fracture patterns), where prognosis for recovery and fixation are of major concern. Currently, there is no a single study that has examined, in a comprehensive way, the morphological and metrical characteristics of fractures in regard to the impact energy of the force applied in a forensic perspective, simulating a situation occurring in pedestrian road traffic accidents.

2. Objective of study

This study has two objectives, to establish a usable fracture analysis method and to reveal the association between the energy of the force and the fracture pattern.

3. Material and methods

Experimental set-up: the Dynatup Model POE 2000 (Instron Co.) low energy pendulum impact machine, shown in Fig. 1, was utilized to apply impact loading on pig femoral bones. Custom-made supports for holding each bone in place during loading were fabricated. The clamp shaft was designed to support the bone while the impact load was oriented in perpendicular to the longitudinal axis of the bone (Fig. 2). The bone clamp shaft was adjusted to position the bone for three-point bending with additional bone compression, simulating body weight on a leg (as in standing position). The compression forces (in relation to the long axis of the bone) were generated by moving the clamp plates located at the edges of the bone; the exact amount of compression forces was adjusted and monitored using the Tension Compression Load Cell (Vishay Tedea-Huntleigh 615) and digital monitor (Rinstrum 310). Two adjustable supports allow the inner loading span along the bone shaft to be altered depending on the bone size (Fig. 2). Bones' preparation: fresh femora of young pigs (5–6 months) were exposed to the impact. Juvenile bones were selected for this study since road traffic injuries are the leading cause of death worldwide among young people aged 10–24 (World Health Organization) [21]. The similarities between pig and human bones, mainly in regard to their shape, microstructure (i.e., Haversian system) [41] and density [1], make the former an excellent model for human bone mass and strength [42]. Immature pigs at their early stage of development manifest a plexiform bone structure (a type of primary bone tissue). Nevertheless, by the age of 5–6 months most of the cortical is of the Haversian type, as in humans. The pig bones were obtained fresh (on the day of slaughter) and almost clean from an abattoir. The specimen preparation included careful separation of remnant muscles and all other soft tissues from the bones, including the periosteum. All bones were visually examined for macroscopic defects, skeletal disease, or pre-fracture, and later were stored frozen at $-20\,^{\circ}$C until testing. The bones were labeled and their length and mid-shaft dimensions were measured. In order to hold the bones stable in the compression clamps so that compression forces will be applied on all articular areas, the bones' epiphyses were embedded in transparent polyester resin (Erco E-16®). Preceding the coating process, the bones were thawed with water to room temperature and stored in a water tank during processing. Four drops of accelerator solution and 3 ml of hardener solution were inserted into a small plastic container containing 120 ml of liquid transparent polyester in order to prepare the polyester solution (the plastic containers were covered on the inside with a thin layer of Vaseline in order to prevent the polyester from sticking). The bones were inserted into the empty plastic container with their longitudinal axis perpendicular to the base of the container and handled in a fume hood, using a stable handle. In order to cover the distal epiphysis with polyester, both condyles, in all tests, were set to meet the bottom of the plastic container (leveling process), the plastic containers were leveled horizontally using a simple level bar. Following the leveling process, the polyester solution was poured into the plastic container and left for 30 min until drying and cooling was complete. Testing procedure: All bones were laterally fractured in three-point bending with additional compression configuration under wet conditions. The inner loading span was adjusted consistently to be 8 cm. The compression force applied along the long bone axis through the clamps was adjusted consistently to be 25 kg (assuming equal compression force on each leg of a 50 kg subject). The bones were set in the compression clamp with their longitudinal axis perpendicular to the pendulum movement. The tup of the pendulum (impact body), a half-cylinder shaped-body (10 mm diameter) made of stainless steel was adjusted to meet the bone in its mid-span point (center of the bone). The longitudinal axis of the tup was oriented perpendicular to the longitudinal axis of the bone, creating a contact-point impact. The energy of the pendulum (in Joules) was calculated based on its potential energy at the initial height where the pendulum was elevated:

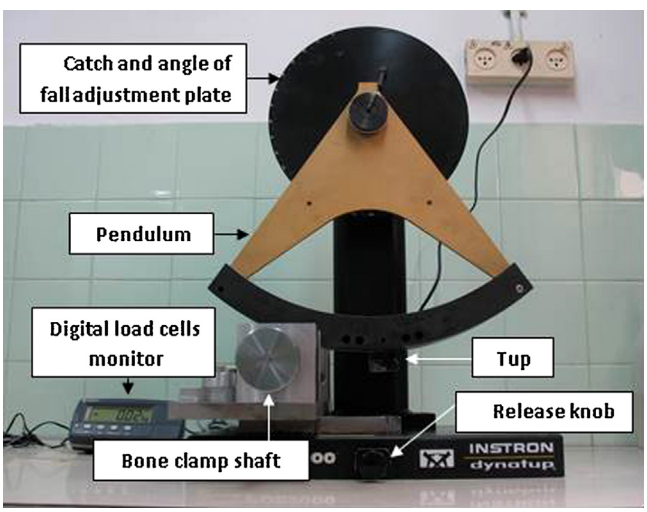

Fig. 1. Instron POE 2000 pendulum machine used in the current study.

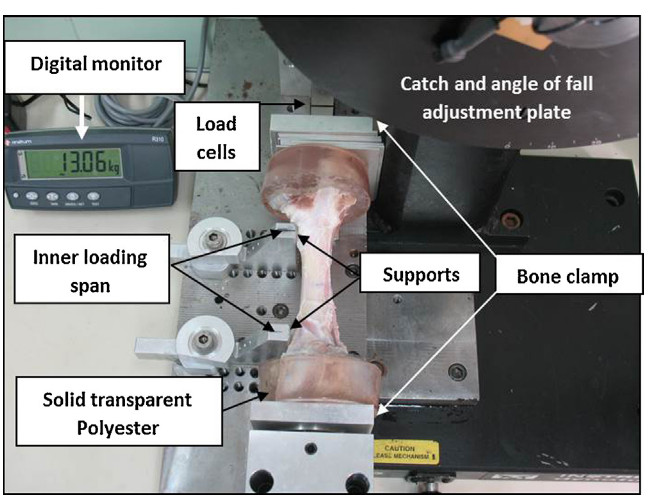

Fig. 2. Bone clamp device. Note that the bone epiphyses are embedded in solid polyester.

$$E_P = mgh \tag{1}$$

where m is the mass (kgm), g (9.81 m/s^2), is the gravity acceleration, h (m) is the height from which the pendulum was released.

The mass (m) and the pendulum height (h) in Eq. (1) were calculated by

$$\begin{aligned} W &= mg \\ h &= L(1-\sin(90-\theta)) \end{aligned} \tag{2}$$

where W is the weight of the body-mass, L is the length of the pendulum arm and θ is the angle of the body-mass elevation.

Table 1
The initial potential energy and velocity at the impact calculated by the angle and the height of the pendulum.

θ	h (m)	E_p (joule)	v (m/s)
70°	0.21	20.6	2.02
120°	0.476	46.7	3.05
160°	0.616	60.4	3.47

The velocity at the impact was calculated by assuming that all the potential energy was transferred into kinetic energy (Table 1). That is:

$$mgh = \frac{1}{2}mv^2 \tag{3}$$

The tests: a custom made impactor-body (tup) was connected to the pendulum. Three different energies were applied by changing the pendulum initial heights and 10 bones were included in each test:

The following three tests were applied:

Test-1: low velocity impact (2.02 m/s).

Test-2: moderate velocity impact (3.05 m/s).

Test-3: high velocity impact (3.47 m/s).

The following independent variables were measured either prior or following testing:

1. **Bone maximum length:** the maximum length between the head of the femur and the condyles. This variable was measured prior to testing.
2. **Cross sectional dimensions at the impact point:** the dimensions were needed for determining the influence of the bending moment of inertia on fracture pattern and were measured using a digital caliper. The external lateral-medial and anterior-posterior dimensions were measured prior testing and the cortical bone thickness was measured following testing. The lateral-medial dimensions were significantly higher (4%; $p < 0.001$) than the anterior-posterior dimensions, hence, the moment of inertia of a tube in bending was considered based on the lateral-medial dimensions only (impact direction) as following:

$$I = \frac{\pi(d_E^4 - d_I^4)}{64} \tag{4}$$

where d_E = external lateral-medial diameter, d_I = internal lateral-medial diameter, $d_I = d_E - (t_i + t_j)$ where:t_i = thickness of the lateral cortex, t_j = thickness of the medial cortex.

The following dependent variables were measured following testing:

1. **Fracture lines:** any fracture line longer than 1 cm was counted. Fracture lines may appear in different forms: longitudinal, oblique, transverse, or polygonal (see below for more details). For each test, the following parameters regarding fracture lines were determined: present or not, their amount, fracture lines location, and their total length (mm). Fracture lines were defined by:
   a. **Longitudinal lines:** straight lines running proximally or distally toward the epiphysis. The longitudinal lines may appear in all aspects of the bone, but usually they appear in the area of impact (C- longitudinal line), in the contralateral aspect (CL- longitudinal line), or in both aspects. Related observations and measurements: presence, number, and location (Fig. 3a).
   b. **Oblique lines:** fracture lines running at an angle to the long axis of the bone. Oblique lines usually run proximally or distally toward the epiphysis and to other aspects of the bone. Although continuous on all bone aspects the oblique lines appeared (e.g., 3-dimensional), for morphological description purposes, oblique fracture lines were defined as such in each aspect of the bone (anterior, posterior, medial, and lateral) (Figs. 3a, d and c).

   Polygonal: these lines were defined if an area on the bone was encircled by two oblique lines. One line is running proximally and one distally from the area of impact, usually toward the contralateral aspect.

   Related observations and measurements: presence, number, location and length (mm) (Fig. 3a).
   c. **Transverse line:** horizontal line fully encircles the diaphysis. It appears straight or fractured. Related measurements: presence (Fig. 3a).
   d. **Curvature index:** number of times the fracture line deviates from its course (Fig. 3b).
2. **Branching points:** a point along a longitudinal line from which two oblique lines branched out. Related measurements: length between the branching points (mm) (Fig. 3c).
3. **Chip fragment:** missing bony part at the point of impact. Related: observations and measurements: presence and circumferential length (mm) (Fig. 3d).

3.1. Bone preparation for fracture lines analysis: post-test procedure

The cleaning process consisted of 5 h of boiling in water with detergent, 20 min soaking in Hydrogen Peroxide 35%, and 10 min rinsing with water (preceding the cleaning process all the polyester coating was removed). All bone fragments were placed on blotting paper and allowed to dry for 24 h. Following the cleaning and drying processes, all bony fragments were reassembled to form a complete bone using UHU adhesive.

3.2. Fracture lines analysis

The quantitative fracture lines analysis was carried out by measuring the fracture lines length using Microscribe® G2X 3D digitizers directly on the reassembled bones. The X, Y, and Z coordinates of the deviation points along each segment of the fracture line were obtained. The length between each pair of points was calculated by 3D Pythagoras Theorem. The total fracture line length was the sum of the segments lengths.

3.3. Statistics

The statistical analysis was carried out using SPSS V15. Descriptive statistics were applied on all data. An ANOVA test was applied to analyze the differences between the group means. A T-test was applied to detect significant differences in parameters means between two groups. A Chi-square test was applied to reveal associations between categorical variables.

A Kruskal–Wallis test was applied to evaluate between-group differences in non-parametric variables. p value was set of $p < 0.05$.

4. Results

This study describes and analyzes fracture pattern in two modes: qualitative and quantitative. In the quantitative mode the fracture measurements are summarized. In the qualitative mode, schematic illustrations of the fracture patterns are presented for each test. Mean values (±SD) of bone and fracture characteristics relating to different impact energy are presented in Table 2. No significant differences in cross-sectional moment of inertia were found between the femora in the three tests carried out. Therefore the upcoming results are due to other factors than morphometrical

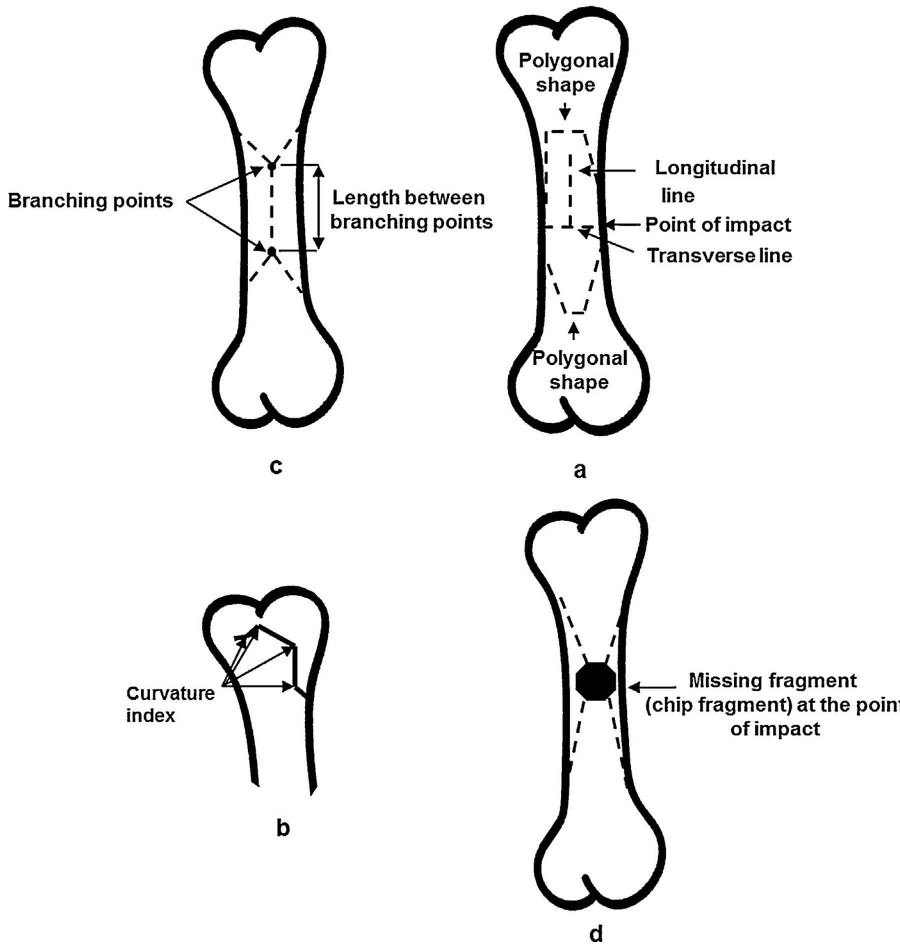

Fig. 3. The fracture lines that were measured following testing. (a) Longitudinal, transverse and oblique line and polygonal shape. (b) Curvature index calculations (in this illustration, the fracture line deviates 4 times from its course). (c) Length between branching points measurement and (d) chip fragment.

Table 2
Bone and fracture parameters under different impact energies ($N = 10$ in each test).

Measurements	Test 1 (T_1) (low energy)		Test 2 (T_2) (moderate energy)		Test 3 (T_3) (high energy)		p value*
	Mean	+SD	Mean	+SD	Mean	+SD	
Bone length (mm)	191.6	9.8	192.1	9.6	199.1	12.3	0.2^A
Cross-sectional moment of inertia (mm^4)	13,252.6	4326.5	12,643.6	2725.1	14,518.8	4563.3	0.5^A
Number of fracture lines	3.2	1.3	7.5	2.4	6.10	1.7	**T_1 vs. T_2^K** **T_1 vs. T_3^K**
Fracture line (polygon) length (mm)	101.1	49.5	416.1	72.2	306.1	121.8	**T_1 vs. T_2^A** **T_1 vs. T_3^A**
Curvature index	3.3	4.5	39.7	8.4	30.90	12.2	**T_1 vs. T_2^K** **T_1 vs. T_3^K**
Chip size (mm)	0	0	32.9	10.2	75.14	19.8	**T_2 vs. T_3^K**

* Statistical significance at $p < 0.05$ (marked in bold).
K – Kruskal–Wallis test; A – one-way ANOVA test.

differences in femur characteristics between the tests. On average, the number of fracture lines created under moderate and high-energy impact is significantly higher (approximately double) than those created by a low-energy impact (7.5 and 6.1 vs. 3.2, respectively, $p < 0.05$). The fracture lines under moderate and high-energy impact compared to low-energy are significantly longer (416.1 mm and 306.1 mm vs. 101.1 mm, respectively, $p < 0.05$) and more curved (curvature index 39.7 and 30.9 vs. 3.3, respectively, $p < 0.05$). No bone chips were found in bones impacted at low energy. Bone chips were significantly larger in bones impacted by a high-energy body (75.4 mm) compared to moderate energy (32.9 mm) ($p < 0.05$). Spearman correlation coefficients between energy, bone parameters, and fracture features are presented in Table 3. Significant positive correlations were found between energy and all fracture parameters; as the energy of the impact increases, the number of fracture lines and their length and curvature index increase. Bone-chip size also increases with impact energy. Significant positive correlations were also found between fracture parameters: as the number of fracture lines increase, their length and curvature index also increase. A strong positive correlation (0.903, $p < 0.001$) was found between the fracture length and the curvature index: the longer the fracture line, the greater the curvature index. No correlations were found between

Table 3
Spearman correlations coefficients between energy of impact, bone features and fracture features ($N = 30$).[*]

Parameters		Number of fracture lines	Fracture length	Curvature index	Chip size
Energy	*r*	**0.473**	**0.542**	**0.596**	**0.608**
	p value	0.008	0.002	0.001	0.001
Bone length	*r*	0.096	**0.377**	0.254	0.102
	p value	0.613	0.040	0.176	0.592
Cross-sectional moment of inertia (mm^4)	*r*	0.111	0.286	0.133	0.083
	p value	0.555	0.126	0.485	0.661
Number of fracture lines	*r*	–	**0.705**	**0.816**	0.012
	p value	–	0.001	0.001	0.918
Fracture length	*r*	–	–	**0.903**	0.158
	p value	–	–	0.001	0.405
Curvature index	*r*	–	–	–	0.157
	p value	–	–	–	0.407

[*] Significant correlations are marked in bold.

bone-chip size and fracture length, number, and curvature index. A positive correlation was found between bone length and fracture length. The results of a non-metric analysis of the fracture parameters obtained in all tests are presented in Tables 4 and 5. A significant association was found between the impact energy and the number of the longitudinal lines and polygons in the area of impact. All bones impacted at low energy manifested longitudinal lines, in the moderate energy impact – only 2 out of 10 bones, in high energy impact – none of the bones exhibited longitudinal lines in the area of impact. In 50% of bones subjected to low-energy impact, the longitudinal lines were located on both the impact and contralateral side, 20% on the impact side only and 30% on the contralateral side only (Table 5). Polygonal fragments (mostly two) were found in 95% of the bones following both moderate- and high-energy impact. No polygons were found in bones following low-energy impact (Table 4). All polygonal fragments in bones following moderate-energy impact were located on the anterior and posterior aspect of the bone; however, in bones subjected to high-energy impact the polygonal fragments were mostly located on the contralateral (medial) aspect (only 30% were located on the anterior and posterior aspects). The average number of fracture lines by impact energy and bone aspect is presented in Table 6. Albeit not significantly, most fractures lines were located on the impacted (lateral) aspect in bones subjected to moderate- and high-velocity impact. In bones subjected to low- and moderate-energy impact, the medial aspect also presents a large number of fracture lines as compared to the anterior and posterior aspect.

5. Summary

A bone fracture following a low-velocity impact can be identified mainly as a simple transverse fracture. The impacted

Table 4
Fracture features under tests 1–3 conditions: non-metric analysis.[a]

Parameter	Test 1 (low energy)		Test 2 (moderate energy)		Test 3 (high energy)		*p* chi-square test
	Pr present	Absent	Pr present	Absent	Pr present	Absent	
C- longitudinal lines	10	0	2	8	0	10	<0.001
Polygons	0	10	10	0	9	1	<0.001

[a] 10 bones were utilized in each test.

Table 5
Number and location of longitudinal lines under different impact energy (tests 1–3).

Parameter	Test 1 (low energy)	Test 2 (moderate energy)	Test 3 (high energy)
Average number of longitudinal lines[a]	2.2	0.2	0
Location of longitudinal lines (aspect)	50% = impact + contralateral 20% = impact 30% = contralateral	100% = contralateral	–

[a] In one bone.

Table 6
Average number of fracture lines by impact energy and bone aspect when lateral side is impacted ($N = 10$ in each group).

Bone aspect energy	Lateral		Anterior		Posterior		Medial		*p* value[a]
	Mean	Std.	Mean	Std.	Mean	Std.	Mean	Std.	
1 – low-energy impact	2.1	1.3	1.7	0.5	2.2	1.6	2.4	1.1	0.750
2 – moderate-energy impact	5.1	2.0	3.3	1.4	3.1	1.2	3.6	1.2	0.060
3 – high-energy impact	4.9	1.8	3.6	1.4	3.2	1.8	3.3	1.6	0.120

[a] Kruskal–Wallis test.

and the contralateral sides are mostly characterized by a short longitudinal line that crosses the transverse fracture toward the epiphyses (on the impacted aspect, the meeting point of the transverse line and longitudinal line is the point of impact). However, a fracture following a moderate- or high-velocity impact results in a comminuted or multifragment double butterfly pattern. The impact side can be identified by the presence of four long oblique-radial lines branching from a chip fragment, creating a cross-shape pattern and running toward the anterior and posterior aspect of the bone. On the anterior aspect, radiating lines run inferiorly or superiorly from the oblique-radial lines toward the transverse line. The contralateral side is characterized by a common edge line running superiorly and inferiorly toward the epiphysis. In bones subjected to a high-velocity impact, the chip fragment appears larger (twice as large) than in bones subjected to a moderate velocity impact. In some cases (20%), the fracture following a moderate velocity impact can be identified by the presence of a short longitudinal line running superiorly form the chip fragment (this longitudinal line is absent in bones subjected to a high-velocity impact).

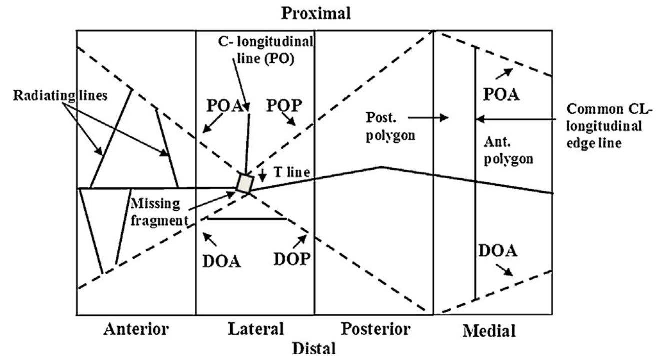

Fig. 5. Schematic illustration of the fracture pattern of moderate velocity impact. Note the missing fragment, the four long oblique lines (POA, proximal oblique anterior, POP, proximal oblique posterior) (DOA, distal oblique anterior, DOP, distal oblique posterior), and the complete transverse line (T line). These oblique lines run posteriorly and anteriorly, eventually forming two polygons (anterior and posterior). The broken lines represent the four long oblique lines and the butterfly fracture on the lateral aspect.

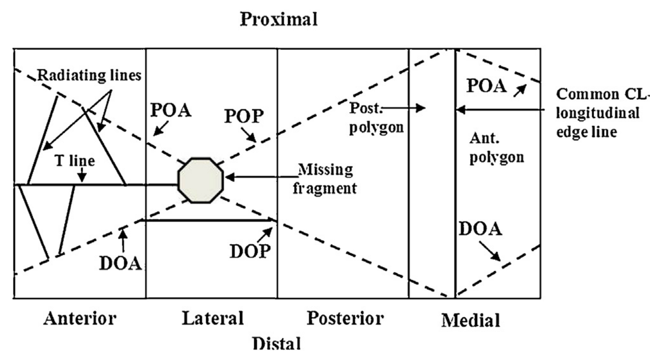

Fig. 6. Schematic illustration of the fracture pattern of high-velocity impact. Note the large missing fragment, the four oblique lines (POA, proximal oblique anterior, POP, proximal oblique posterior) (DOA, distal oblique anterior, DOP, distal oblique posterior), and the incomplete T line. These oblique lines run posteriorly and anteriorly, eventually forming two polygons. The broken lines represent the four long oblique lines and the butterfly fracture on the lateral aspect.

6. Discussion

In the current study, a complete transverse fracture is observed in bones subjected to a low-velocity impact, but although expected, the butterfly pattern is absent (Fig. 4) [4]. In bones exposed to a moderate- or high-velocity impact, the fracture pattern becomes significantly more comminuted as was found previously [4] and is characterized by a greater number of longer fracture lines, in particular, on the impacted (lateral) aspect (Figs. 5 and 6). A larger chip fragment is also present in bones exposed to a moderate- or high-velocity impact at the point of impact, accompanying the transverse line. In the case of a low-energy impact, the presence of a transverse line with only a few accompanying longitudinal lines indicates great internal tension forces governing the fracture [11]. In bones subjected to a moderate velocity impact, other major fracture lines accompany the transverse line, indicating additional internal shearing forces developing in the bone that eventually create the butterfly pattern. As reported, the transverse line becomes incomplete as the velocity increases [9] and they are located mostly on the impact aspect indicating even greater shear forces than tension forces. Compared to bones exposed to a low-velocity impact, in bones exposed to a moderate- or high-velocity impact, four major oblique lines (POA, POP, DOA and DOP) are present (see Figs. 5 and 6). In other studies analyzing fracture patterns, these oblique lines are sometimes called radial fractures, as they originate from a common point [43] or cone cracks [28]. In our study, the oblique lines are seen running from the point of impact, creating a double butterfly pattern accompanying the transverse fracture. The butterfly fractures of each side extend to the opposite side of the bone, ultimately coming in contact with one another to form a longitudinal fracture ("common CL- longitudinal edge line") on the opposite side, completing the double butterfly fracture pattern. The oblique lines represent the shear stresses developing at a plane that is at approximately 45° to the long axis of the bone [45]. Oblique fracture lines also result from a combination of torsion and bending when bending is the dominant loading [4]. One possible explanation for the additional and longer oblique fracture lines following moderate- and high-velocity impact is that a larger amount of energy needs to be dissipated through the fracture of the bone as the energy increases. In the case of a low-velocity impact, most fracture lines are seen in all aspects of the bone (see Fig. 4). In the case of a moderate- or high-velocity impact, although not significantly so, most fracture lines are seen mostly on the impacted (lateral) aspect (see Figs. 5 and 6). The applied energy has to dissipate within the bone. It can be assumed that in cases of low velocity impact the bone can be deformed and the energy dissipates toward the anterior and posterior aspects and the contralateral aspect where tensile stresses develop. However, with

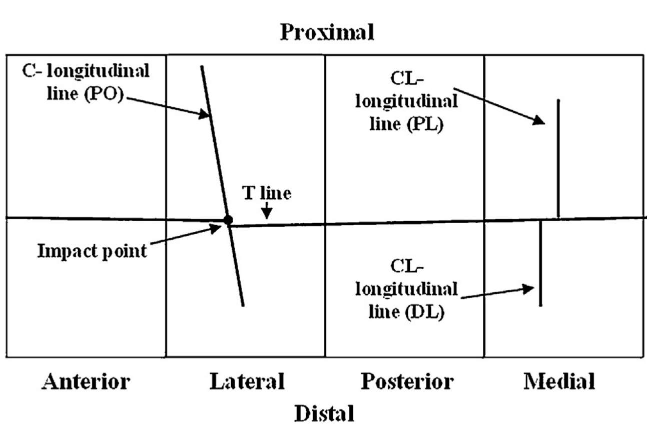

Fig. 4. Schematic illustration of the fracture pattern under low-velocity impact. Note the transverse line (T line), the formation of the longitudinal line in the area of impact (C- longitudinal line) and in the contralateral aspect (CL- longitudinal line). The chip fragment is missing at the point of impact.

moderate and high velocity impacts, the bone behaves more like brittle material and once the impactor transfers the energy to the bone – no bone deformation occurs and fracture develops. It is worth noting that although the size of the impactor remains constant, the size of the chip fragments at the point of impact increases with the velocity of the impact. Therefore, according to this study, it is possible to identify the point of impact, but not the size of the impactor, according the location of the chip fragment. All fracture parameters were found to be greater in bones subjected to a moderate- and high-velocity impact than in those subjected to low-velocity impact. The difference between the low and moderate velocity impact is 1.03 m/s as compared to 0.41 m/s between the moderate and high velocity impact. This could explain the large and significant morphological differences between fractures following low and moderate/high-velocity impacts, and the small morphological differences between fractures following moderate- and high-velocity impacts. Torsion also creates a state of pure shear between parallel transverse planes and maximum tensile stresses develop at a 45° to the longitudinal axis [17]. Spiral fracture caused by torsion is also characterized by a vertical segment, which is the last component to form [10]. In the current study, this vertical segment is expressed as the "common CL- longitudinal edge line" on the contralateral side of the bones subjected to a moderate- or high-velocity impact (see Figs. 5 and 6). It is possible that during bending as a result of the impact, the bones that were not fixed to the clamp rotated, producing a vertical segment. In the current study a "true" butterfly fragment that points in the direction of the impact is absent in all cases. Although butterfly fractures are commonly seen in the lower extremities when the thigh or calf receives a lateral blow during weight bearing, as in the case of pedestrians injured by vehicles [10], there is no consensus in the literature with regard to its formation. In the case of a "false" wedge-shaped fragment, the apex, and not the base, is directed toward the impact site, as is shown in this study by the two oblique lines running on the lateral side from the point of impact superiorly and inferiorly toward the contralateral side (DOA and POA or DOP and POP) (see Figs. 5 and 6). Accepting that bone is weaker in tension than compression, one would expect to find a transverse fracture line originating on the contralateral side of impact and a "true" butterfly pattern following bending. In this study, however, although a transverse line is usually present, no "true" butterfly pattern was identified. The four oblique lines seen are running from the point of impact toward the epiphyses, creating a double "false" butterfly pattern. These lines further embrace the metaphyseal area and meet at the contralateral side at a point along the longitudinal fracture line ('common CL-longitudinal edge line'). This "false" double butterfly configuration is commonly seen in long bones following a low-velocity gunshot [28,44]. In our study, the head of the pendulum tup (impact body) was round (10 mm diameter) implying (as in cases with bullets) a very small contact area with the impacted bone. The outcome is a high contact stresses. During a fast-loaded (high-velocity) force, no sufficient tension and bending are developed and the bone reacts as a brittle substance and shatters. The consequence is a V-shape radiating fractures, as failure first occurs at the impact site [26]. This is consistent with studies on vehicle-pedestrian accident, claiming that a "false" wedge-shaped fracture is more common in cases where the area of contact between the limb and the vehicle elements was very small [18,21] (cited from Teresinski [15]).

7. Conclusions

This study, to the best of our knowledge, is the first to examine experimentally variant fracture features in relation to the energy of the force applied, from a forensic perspective. Reconstructing an injury scenario can be complicated especially in cases of comminuted and non-characteristic fractures. In this study, new and significant correlations between fracture pattern and impact characteristics were found. This can serve as a core principle for future studies and forensic case analysis. In this study, a basic model for fracture analysis is presented, the procedures that can to be followed, the different conditions under which the test can be carried out, the means for analyzing the fracture pattern, and finally, the terminology that can be used in future research.

8. Limitations of the study

This study is sample-specific and further validation (independent laboratory and sample) is required in order to develop an appropriate prediction model for bones in general and human bones in particular. For the case of simplicity, bones were impacted at mid-shaft. Other sites of impact may yield different results. Finally, the setting itself bears on the results, i.e., the direction of impact simulated by the Instron apparatus was applied perpendicular to the bone diaphysis hence, different impact direction might result in different fracture pattern.

Acknowledgments

Grant sponsors: Dan David Foundation, Tassia and Dr. Joseph Meychan Chair for the History and Philosophy of Medicine.

References

[1] S.N. Byers, Introduction to Forensic Anthropology, 2nd ed., Pearson Education, 2005.
[2] H.E. Berryman, S.A. Symes, Recognizing gunshot and blunt cranial trauma through fracture interpretation, in: K.J. Reichs (Ed.), Forensic Osteology: Advances in the Identification of Human Remains, Charles C. Thomas, Springfield, IL, 1998, p. 335.
[3] J.K. Reichs, W.M. Bass, Forensic Osteology: Advances in the Identification of Human Remains, 2nd ed., Charles C. Thomas, 1998, p. 333.
[4] J. Rich, D.E. Dean, R.H. Powers, Forensic Medicine of the Lower Extremity, The Humana Press Inc., Totowa, NJ, 2005.
[5] T.A. Kress, D.J. Porta, J.N. Snider, P.M. Fuller, J.P. Paihogios, W.L. Heck, S.J. Frick, J.F. Wasserman, Fracture patterns of human cadaver long bones, in: International Research Council on the Biomechanics of Impact, 1995, 155–169.
[6] I.L. Gitajn, E.K. Rodriguez, Biomechanics of musculoskeletal injury, in: Biomechanics in Applications, InTech, 2011.
[7] A. Galloway, Broken Bones: Anthropological Analysis of Blunt Force Trauma, Charles C. Thomas Publisher Ltd., 1999.
[8] L.F. Rogers, 2nd ed., Radiology of Skeletal Trauma, vol. 1, Churchill Livingstone Inc., New York, 1992.
[9] M.C. Pierce, G.E. Bertocci, E. Vogeley, M.S. Moreland, Evaluating long bone fractures in children: a biomechanical approach with illustrative cases, Child Abuse Negl. 28 (2004) 505–524.
[10] E.R. Gozna, Biomechanics of Musculoskeletal Injury, Williams & Wilkins, Baltimore, 1982.
[11] C.A. Rockwood, D.P. Green, R.W. Bucholz, Fracture in Adults, 7th ed., Lippincott Williams & Wilkins, 2010.
[12] W.U. Spitz, S.F. Russell, The road traffic victim, in: Medicolegal Investigation of Death: Guidelines for the Application of Pathology to Crime Investigation, 2nd ed., Thomas Books, Illinois, 1980, pp. 377–405.
[13] R.S. Levine, An Introduction to Lower Limb Injuries in Biomechanics and Medical Aspects of Lower Limb Injuries, SAE Technical Paper #861922, Society of Automotive Engineers, Inc., 1986, pp. 23–29.
[14] T.R. Reilly, A.H. Burstein, The mechanical properties of cortical bone, J. Bone Jt. Surg. Am. 56 (1974) 1001–1022.
[15] G. Teresinski, R. Mydro, The evidential value of wedge-shaped tibial and femoral fractures in cases of car-to-pedestrian collisions, Probl. Forensic Sci. 40 (XL) (1999) 72–85.
[16] O.U. Messerer, Elasticitat und Festigkeit der menschlichen Knochen, Cotta, Stuttgart, 1880, pp. 1–100.
[17] C.H. Turner, D.B. Burr, Basic biomechanical measurements of bone: a tutorial, Bone 14 (1993) 595–608.
[18] H. Patscheider, Über Anprallverletzungen der unteren Gliedmaßen bei Straßenverkehrsunfällen, Dtsch. Z. Gerichtl. Med. 54 (S) (1963) 336–366.
[20] S.N. Kozlov, A.G. Yurasow, Neprjamye perelomy bedra pri udare bamperom avtomobilja, Sudebno-Med. Ekspert. XXIV (1981) 13–15.
[21] O. Prokop, Forensische Medizin, VEB Verlag Volk, Berlin, 1966.
[22] J.J. Eubanks, P.F. Hill, Pedestrian Accident Reconstruction and Litigation, Lawyers & Judges Publishing Co., 1999.
[23] W. Dürwald, Gerichtsmedizinische Untersuchungen bei Verkehrsunfällen, Thieme: VEB Georg, Leipzig, 1966.

[24] W.U. Spitz, R.S. Fisher, Medicolegal Investigation of Death, 3rd ed., Charles C. Thomas, Springfield, 1993.
[25] B. Karger, K. Teige, M. Fuchs, B. Brinkmann, Was the pedestrian hit in an erect position before being run over? Forensic Sci. Int. 119 (2001) 217–220.
[26] D. Dirkmaat, Interpreting traumatic injury to bone in medicolegal investigations, in: A Companion to Forensic Anthropology, 1st ed., Blackwell Publishing Ltd., 2012.
[27] World Health Organization, Internet site: http://www.who.int/features/factfiles/youth_roadsafety/en/index.html.
[28] D.C. Kieser, R. Riddell, J.A. Kieser, J.C. Theis, M.V. Swain, Bone micro-fracture observations from direct impact of slow velocity projectiles, J. Arch. Mil. Med. 2 (1) (2014) e15614.
[29] R.S. Levine, Injury to the extremities, in: A.M. Nahum, J.W. Melvin (Eds.), Accidental Injury, Springer-Verlag, New York, 2002, pp. 491–522.
[30] M.A. Gomez, A.M. Nahum, Biomechanics of bone, in: A.M. Nahum, J.W. Melvin (Eds.), Accidental Injury, Springer-Verlag, New York, 2002, pp. p.206–p.227.
[31] K. Sellier, Zur mechanic des knochenbruchs, Dtsch. Z. Gerichtl. Med. 56 (1965) 341–348.
[32] J.K. Mason, B.N. Purdue, The Pathology of Trauma, 3rd ed., Arnold Publishing, London, 2000.
[33] R.J. Brumback, The rationales of interlocking nailing of the femur, tibia, and humerus, Clin. Orthop. Relat. Res. 324 (1996) 292–320.
[34] J.W. Harkess, Principles of fractures and dislocations, in: C.A. Rockwood, D.P. Green (Eds.), Fractures, J.B. Lippincott, Philadelphia, 1975.
[35] P. Ducheyne, M. Martens, D.P. Meester, E. Aemoudt, M. Vrancken, H.F. Van, J.C. Mulier, Microscopic fracture aspects of impact tested human bones, J. Bioeng. 1 (1977) 197–207.
[36] V. Ebacher, H. Tang, H. McKay, T. Oxland, P. Guy, R. Wang, Strain redistribution and cracking behavior of human bone during bending, Bone 40 (2007) 1265–1275.
[37] E.G. Fantner, H. Birkedal, J. Kindt, T. Hassenkam, J. Weaver, J. Cutroni, B. Bosma, L. Bawazer, M. Finch, G. Cidade, Influence of the degradation of the organic matrix on the microscopic fracture behavior of trabecular bone, Bone 35 (2004) 1013–1022.
[38] K.A. Nalla, J.S. Stolken, J.H. Kinney, R.O. Ritchie, Fracture in human cortical bone: local fracture criteria and toughening mechanism, J. Biomech. 38 (2005) 1517–1525.
[39] G.C. Reill, J.D. Currey, The effects of damage and microcracking on the impact strength of bone, J. Biomech. 33 (2000) 337–343.
[40] B.D. Browner, Skeletal Trauma, 4th ed., W.B. Saunders Company, 2009.
[41] M.E. Hillier, L.S. Bell, Differentiating human bone from animal bone: a review of histological methods, J. Forensic Sci. 52 (2007) 249–263.
[42] W. Pond, K. Houpt, The Biology of the Pig, 1st ed., Comstock Publishing Associates, Ithaca, NY, 1978.
[43] C.G. Knight, M.V. Swain, M.M. Chaudhri, Impact of small steel spheres on glass surfaces, J. Mater. Sci. 12 (8) (1977) 1573–1586.
[44] J.R. Ryan, R.T. Hensel, G.G. Salciccioli, H.E. Pedersen, Factures of the femur secondary to low-velocity gunshot wounds, J. Trauma 21 (2) (1981) 160–162.
[45] J. Aerssens, S. Boonen, G. Lowet, J. Dequeker, Interspecies differences in bone composition, density, and quality: potential implications for in vivo bone research, Endocrinology 139 (1998) 663–670.